Planetary and Space Science 119 (2015) 48–53

Contents lists available at ScienceDirect

Planetary and Space Science

journal homepage: www.elsevier.com/locate/pss

Oxygen foreshock of Mars

M. Yamauchi [a,*], R. Lundin [b], R.A. Frahm [c], J.-A. Sauvaud [d], M. Holmström [a], S. Barabash [a]

[a] Swedish Institute of Space Physics (IRF), Box 812, SE-98128 Kiruna, Sweden
[b] Swedish Institute of Space Physics (IRF), Teknikhuset, SE-90187 Umeå, Sweden
[c] Southwest Research Institute, 6220 Culebra Road, San Antonio, TX 78238, USA
[d] Institut de Recherche en Astrophysique et Planetologie (IRAP), CNRS/Université de Toulouse, 9 avenue du Colonel Roche, BP 44346, F-31028 Toulouse, Cedex 4 France

ARTICLE INFO

Article history:
Received 16 February 2015
Received in revised form
28 July 2015
Accepted 3 August 2015
Available online 19 August 2015

Keywords:
Foreshock
Mars Express
Oxygen
Bow shock electric field
Solar wind reflection
Ion escape
ASPERA-3

ABSTRACT

Mars Express (MEX) has operated for more than 10 years in the environment of Mars, providing solar wind ion observations from the Analyzer of Space Plasmas and Energetic Atoms experiment's Ion Mass Analyser (IMA). On 21 September 2008, MEX/IMA detected foreshock-like discrete distributions of oxygen ions at around 1 keV in the solar wind attached to the bow shock and this distribution was observed continuously up to more than 2000 km from the bow shock. Foreshock-like protons are also observed but at a shifted location from the oxygen by about 1000 km, at a slightly higher energy, and flowing in a slightly different direction than the oxygen ions. Both protons and oxygen ions are flowing anti-sunward at different angles with respect to the solar wind direction. This is the first time that a substantial amount of planetary oxygen is observed upstream of the bow shock. Although rare, this is not the only IMA observation of foreshock-like oxygen: oxygen ions are sometimes observed for a short period of time (<5 min) inside the foreshock region. These observations suggest a new escape channel for planetary ions through the acceleration in the bow shock–magnetosheath region.

1. Introduction

In the solar wind where the interplanetary magnetic field (IMF) points toward the bow shock, a region of ions flowing away from the bow shock with energy higher than the solar wind is sometimes formed (e.g., Asbridge et al., 1968; Eastwood et al., 2005). This phenomenon is the foreshock. Besides the solar wind, there are two types of foreshock ions: high-energy ions with diffuse pitch angle–energy distributions and low-energy ions (up to about 6 times the solar wind energy) with discrete pitch angle–energy distributions. The latter is further subdivided into field-aligned ion beams and gyrating ion flow (Eastwood et al., 2005; Yamauchi et al., 2011). In this paper we consider only the discrete component. The He^{++}/H^{+} ratio of foreshock ions upstream of the Earth's bow shock is lower than the ratio in the solar wind or magnetosheath (Fuselier and Thomsen, 1992). For the magnetospheric component, AMPTE/CCE spacecraft detected energetic O^{+} of more than 40 keV inside the foreshock (Möbius et al., 1986; Krimigis et al., 1986). However, they are interpreted as either the diffuse component that went though the Fermi acceleration inside the bow shock (Möbius et al., 1986) or leakage from the magnetosphere (Edmiston et al., 1982; Krimigis et al., 1986; Sarris et al., 1987; Sibeck et al., 1988). Foreshocks with a discrete component of O^{+} at several keV have never been detected.

The probability of observing foreshocks is different for different planets or objects: they are often observed upstream of the terrestrial and Venus bow shocks, but seldom observed upstream of the Martian bow shock. Phobos-2 observed the foreshock signatures upstream of the Martian bow shock (Dubinin et al., 2000); however, using the Mars Express (MEX) ion mass analyser (IMA) data for the 2004–2005 period, we could not find ion distributions similar to the foreshock ions of the Earth or Venus (Yamauchi et al., 2011) in the dayside upstream region of Mars.

Instead, MEX/IMA detected reflected ions and tailward ion flow, just outside of the bow shock. These ions form a double foot structure outside the bow shock. The first layer (foot) at very close to the bow shock boundary (within about an ion inertia length) is associated with a tailward directed collimated ion flow along the bow shock surface. The second layer is associated with reflected solar wind protons. These reflected solar wind protons continually return to the bow shock for another reflection after gyrating around the interplanetary magnetic field (IMF) (Yamauchi et al., 2011). Such a multiple reflection signature has not been found at Venus, although this could be due to the spatial resolution of the observation (Venus Express traverses the bow shock very quickly compared to MEX). Yamauchi et al. (2011) suggested that the

* Corresponding author. Tel.: +46 980 79120; fax: +46 980 79050.
E-mail address: M.Yamauchi@irf.se (M. Yamauchi).

http://dx.doi.org/10.1016/j.pss.2015.08.003

difference between Venus and Mars comes from the curvature of the bow shock compared to the local ion gyroradius and from the existence of cold ions inside the bow shock (Dubinin et al., 1993).

Although the reflection is considered as a possible mechanism for generating the discrete component of foreshock ions (Gosling et al., 1978; Paschmann et al., 1980; Kucharek et al., 2004), Yamauchi et al. (2011) did not call the reflected ion signature foreshock because (1) the ion distribution was more discrete than ordinary foreshock ions observed at the Earth or Venus, (2) the region where these ions were found was limited to be close to the bow shock, (3) the exact mechanism for reflection still remained as an open question, and (4) foreshock ions might still be formed by mechanisms other than the reflection of the solar wind.

Yamauchi et al. (2012) identified nine cases between 2004 and 2005 where the ion distribution in the foreshock region showed a triple ring structure. The lowest energy ring represents gyromotion around the IMF of pick-up ions that originate from newly ionized exospheric hydrogen. The two extra rings at higher energy represent gyromotion of multiply reflected ions (first and second bounces) around the IMF. The velocity distribution of the pick-up ions was used to identify the magnetic field orientation. The analyses revealed that the reflections could be specular, i.e., without gyration of ions during the trajectory from entering into the bow shock to exiting from the bow shock. Such reflections, i.e., outward accelerations, are possible by an outward directed potential electric field at the bow shock. Since all cases took place at the bow shock flank where the solar wind angle to the bow shock surface is shallow, a strong electric field is not required to reflect 1 keV protons.

On the other hand, many past observations (including those described above) do not exclude local acceleration of ambient ions inside the bow shock–magnetosheath region as an alternative mechanism of forming the foreshock ions, such as wave–particle interactions (Tanaka et al., 1983; Mazelle et al., 2003; Meziane et al., 2004). If cold ions exist inside this acceleration region (in the bow shock–magnetosheath), its behavior could give hint to the acceleration mechanism because potential acceleration energizes cold ions whereas Lorentz force acceleration will not. The Martian bow shock is a good candidate for holding such cold ions (Dubinin et al., 1993), originating from ionized exospheric atoms (coronas). Since the foreshock acceleration mechanism must equally influence such cold ions as well as the solar wind, the cold ion (particularly if it is oxygen) provides extra information about the foreshock acceleration mechanisms.

On 21 September 2008, MEX/IMA detected foreshock-like oxygen ions (O^+) at around 1 keV as intense as protons (H^+), and extending outward from the dayside bow shock. This is the first time that intense O^+ at that energy is observed upstream of the dayside bow shock, including the other planets (for Earth the energy would be much higher). The observation also indicates for the first time that a substantial amount of low-energy O^+ may exist at the bow shock location of Mars. Furthermore, the O^+–H^+ difference provides new information on the acceleration mechanism of the foreshock.

2. Instrument

MEX carries one ion instrument (IMA) and one electron instrument (Electron Spectrometer: ELS). IMA measures ions below 30 keV/q in a 96 step energy sweep every 12 s. The low energy limit and scaling had changed several times during the mission, but the energy stepping above 50 eV remained logarithmic. ELS covers an energy range from 0.5 eV to 20 keV and has several different measurement modes. For the data presented in this paper, ELS measures electrons logarithmically in a 127 step energy sweep every 4 s. Both IMA and ELS are top–hat instruments with a 360° field of view, divided into 16 azimuthal sectors (0–15), each 22.5° wide. The angular acceptance width at the entrance is 4.6° for IMA and 4° for ELS. After completion of each energy scan, IMA also steps the entrance direction, which ranges from −45° to +45° (elevations 0–15) in 192 s using an electrostatic deflection system. Unfortunately, some of IMA's field-of-view (FOV) is blocked by the spacecraft and disappearance of expected counts in the IMF's FOV could sometimes be due to this blockage.

IMA has three mass-resolution modes for detecting different ion species up to 40 amu/q. These three modes have completely different low-energy limits that can detect low-energy protons (the lowest mass-resolution mode is the most favorable for proton detection). For details of the IMA and ELS instruments, see Barabash et al. (2006), Fedorov et al. (2006), and Frahm et al. (2006a, 2006b).

3. Observation

Fig. 1 shows the IMA and ELS observations (energy–time spectrograms) of the outbound traversal of the bow shock from the ionosphere to the solar wind on 21 September 2008. Fig. 2 shows the spacecraft trajectory that corresponds to Fig. 1, indicating that the spacecraft traversed the bow shock nearly radially outward during this bow shock crossing. Fig. 3 shows IMA's FOV at around 01:40 UT of this traversal. From around 01:15 UT to around 01:20 UT, the solar wind was nearly entirely blocked by the spacecraft, and this blockage diminished as the spacecraft moved away from pericenter. Therefore, one may not discuss the intensity of the solar wind for this traversal.

The top two panels of Fig. 1 show the average energy flux accumulated from all azimuthal sectors for the electrons and ions. The lower panels of Fig. 1 show count rates of protons (upper four panels) and heavy ions (lower four panels) from neighboring azimuthal sectors (sectors are common for the protons and heavy

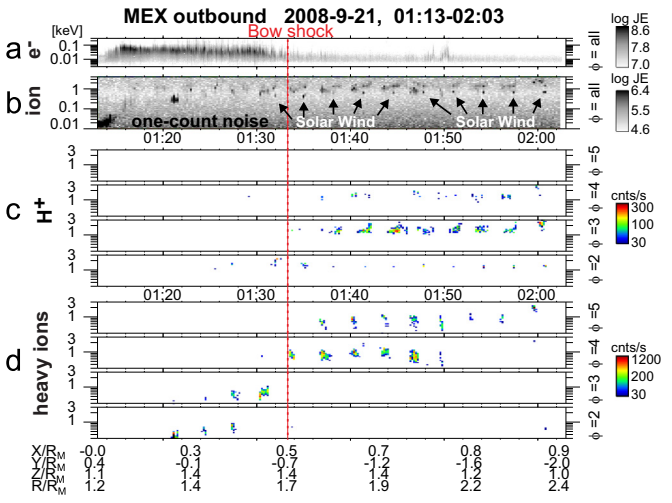

Fig. 1. Observations of foreshock ions during 21 September 2008. Energy–time spectrograms of energy flux (keV cm^{-2} s^{-1} keV^{-1}) for (a) total electron and (b) total ions, and count rate for (c) H^+ at different azimuthal sectors and (d) O^+ at different azimuthal sectors observed by ELS and IMA. Note that this paper uses numbering of 0–15 in the same order as Yamauchi et al. (2006, 2008, 2011, 2012) but some papers used numbering of 1–16. The nearly 3 min (192 s) cycle in the IMA data is due to the scanning cycle in the elevation direction from −45° to +45°. Solar wind protons are observed at around 0.6 keV near 0° elevation angle. The unit R_M is the Mars radius (3397 km). A short burst of electron at around 01:50 UT is consistent with a direct magnetic connection to the bow shock during this short period.

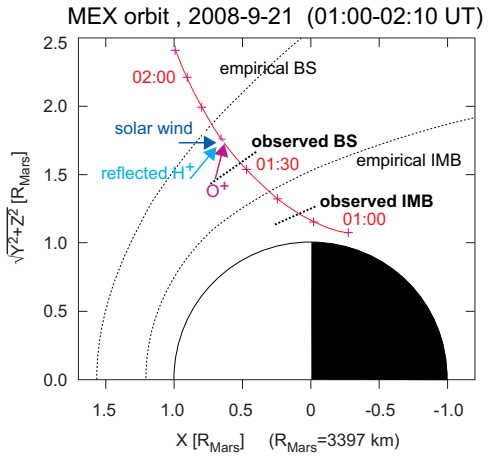

Fig. 2. Orbit of Mars Express during period corresponding to Fig. 1. Time markers are drawn every 10 min with UT hours labeled. Cylindrical coordinates in Mars Solar Orbital (vertical axis denotes the distance from the Sun–Mars line) are used to show the trajectory of the spacecraft in the Mars environment. The thin dashed lines indicate the average position of the bow shock (BS) and ionopause (IMB), respectively, and the Sun is at the left. The solid arrows denote directions exhibiting the most intense flux of the solar wind, foreshock H^+ and O^+.

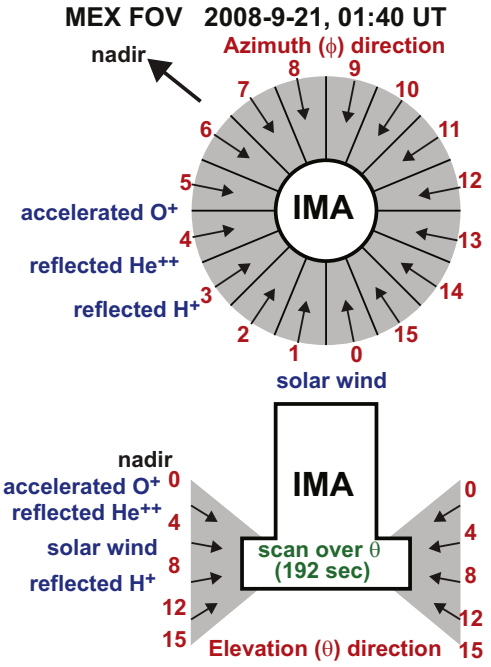

Fig. 3. Definition of field-of-view directions (azimuth and elevation) of IMA. The azimuthal sector numbers (ϕ) are given in the upper panel, and the elevation numbers (θ) are given in the lower panel.

(oxygen) ions). The masses of these ions are confirmed by examining the energy–mass matrix (e.g., Fig. 4a for 01:39–01:42 UT). In the ion data of Fig. 1, the entrance direction of IMA is scanned from $-45°$ to $+45°$ every 192 s, and this is why the ion patterns (particularly the solar wind at 0.6 keV) repeat every 192 s.

At the beginning of the pass, low-energy planetary ions were observed inside the dayside ionosphere, which was identified by photoelectron peaks (strongest one is at around 15 eV in Fig. 1a) before 01:14 UT corresponding to atmospheric CO_2 and O ionization (Frahm et al., 2006a). From about 01:15 UT the shocked electrons were detected until 01:33 UT when the bow shock was crossed. After the bow shock, both intensity and average energy of electrons decreased from 01:31 UT to 01:37 UT. During the same period, solar wind proton energy (0.6 keV in Fig. 1b after 01:37 UT) was observed to decrease to 0.4 keV (01:32 UT and 01:35 UT). Therefore, the ion signature suggests that bow shock boundary is located somewhere between 01:31 and 01:37 UT. Starting from inside the magnetosheath (01:21 UT), through the bow shock, and into the solar wind, a discrete ion population with energy higher than the solar wind energy (0.7–2 keV) is continually observed. This population is detected until the end of instrument operation for this pass (02:02 UT), which corresponds to about 3000 km from the bow shock.

The energy–angle distribution of this discrete ion population, particularly its spread over different directions, is quite different from those of multiple ring distributions that were reported in Yamauchi et al. (2011, 2012). The distribution rather resembles those of ordinary foreshock ions at Venus that is detected using an identical IMA instrument (Yamauchi et al., 2011). Thus, there are two types of discrete ion populations outside the bow shock: one is this foreshock-like structure and the other is the multiple reflection signature.

One outstanding feature of this discrete foreshock event is that it contains O^+. In the oxygen (heavy ion) panels of Fig. 1, discrete O^+ signatures are observed without a corresponding H^+ signature at around 0.7–1 keV during 01:33–01:50 UT in sector 4, and this extends to inside the magnetosheath (01:21 UT) at around 0.3–0.5 keV in sectors 2 and 3, whereas faint signatures (compared to H^+) are observed in sector 5 extending up to the end of the observation interval (02:00 UT). The proton foreshock is also observed at slightly higher energy and in a different direction compared to O^+. The foreshock H^+ are observed at around 1.2–1.4 keV during 01:35–01:57 UT in sector 3, about one and a half-minute after O^+ (i.e., about 35–40° difference in the elevation angle) and above 2 keV in sector 3 at 02:00 UT. Although we cannot quantify the H^+ flux due to the limitation of the instrument and because the proton counts fall un-designated mass channels, the energy flux density is most likely higher for the O^+ foreshock than H^+ foreshock according to Fig. 1b (we can use integration of all mass channel for this purpose because no other species exist for that specific energy and angle). Therefore, the density of the foreshock O^+ is more likely higher than that of the foreshock H^+.

The flow directions of both H^+ and O^+ are narrow and persistent (less than 15° spread from the center direction for 30 min, i.e., more than 2000 km), with H^+ foreshock ions flowing about 50–60° away from the solar wind direction and the O^+ foreshock ions flowing about 70–80° from the solar wind direction, as illustrated in Figs. 2 and 5a. The narrow and persistent direction over a proton gyroradius (normally less than 1000 km) inside the solar wind electric field suggests that the proton flow directions are not far from the IMF direction, because otherwise these ions must occupy wider azimuth-elevation area due to the change of direction during gyromotion (cf. Yamauchi et al., 2012, Figure 3b).

Fig. 1 also indicates that the energy of foreshock O^+ began to rise inside the magnetosheath (01:21 UT) and the most intense flux of O^+ ended at 01:47 UT, whereas foreshock H^+ appeared after (outside the bow shock) and its flux peaked at 02:00 UT. Unlike the solar wind, the absence of foreshock H^+ inside the magnetosheath along the MEX trajectory is not due to the blockage IMA's FOV. Considering the flow angle of these O^+ foreshock ions (about 100 km/s) and H^+ foreshock ions (about 450–600 km/s) they must have come from different locations when these ions left the bow shock as illustrated in Fig. 5a.

In fact, only foreshock O^+ are observed inside the magnetosheath, with its energy gradually increasing from 0.3 keV at 01:21 UT to about 1 keV at 01:33 UT. Considering the short travel time (0.3 keV O^+ travels 2000 km within 40 s), this energy dispersion indicates a long-lasting, accelerating, spatial structure. The short travel time of the foreshock ions indicates that the co-

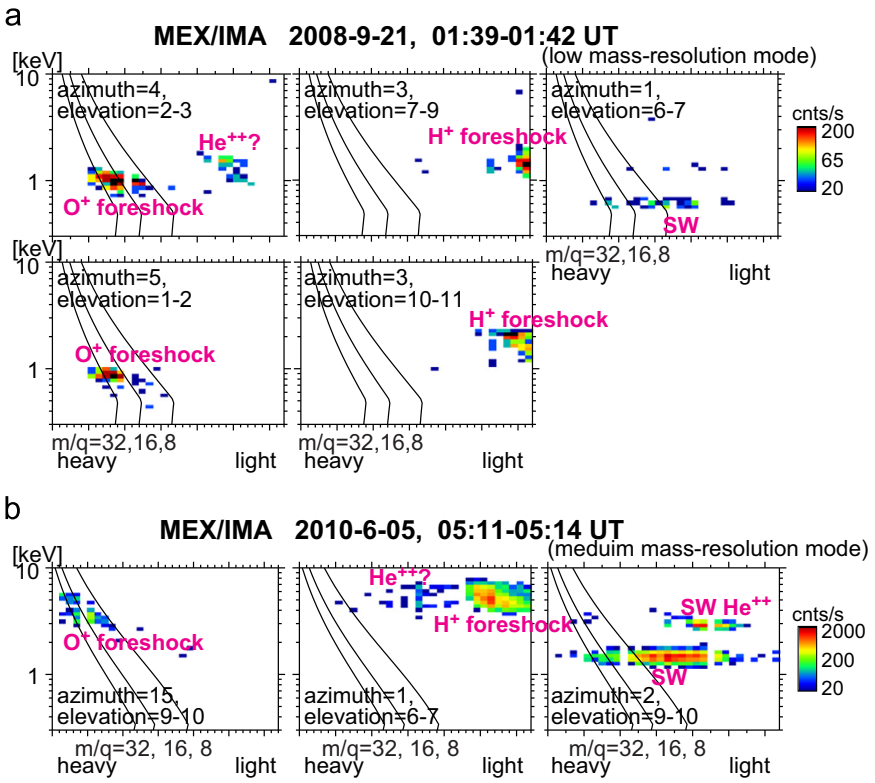

Fig. 4. Energy–mass matrix from one elevation scan (192 s) during the foreshock events showing different ion species on (a) 21 September 2008 and (b) 5 June 2010. Azimuthal/elevation sectors that registered the highest count for each ion species are selected. The solid lines denote expected anode locations (mass channels) at different energies for O_2^+, O^+, and O^{++}. The difference in the location of the expected mass lines between (a) and (b) comes from different mass-resolution mode: (a) medium mass-resolution mode and (b) low mass-resolution mode. The solar wind protons with energy less than 1 keV are reflected from the container of the instrument and are spread across the sensor, scattering across a wide range of mass channels. They are marked as SW. In the He^{++} channel at a different energy and direction from the solar wind He^{++}, an additional He^{++} (marked with "?") signature is observed. This could be reflected solar wind He^{++} although we do not have clear interpretation of why the energy is the same as foreshock H^+.

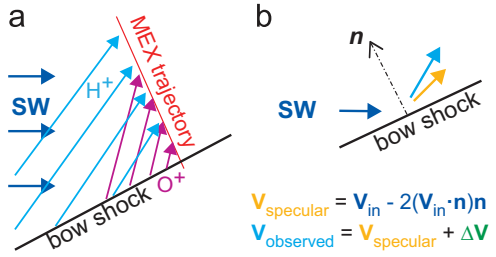

Fig. 5. Illustration of solar wind reflection at the bow shock. The incident solar wind is marked by SW. (a) The direction of observed foreshock ions is mapped back to the bow shock. (b) The directions of specular reflected solar wind at the bow shock (normal direction: ***n***) and the observed foreshock H^+ direction. The difference in the velocity is consistent with velocity of foreshock O^+.

existence of O^+ and H^+ inside the foreshock during 01:38–01:50 UT was simultaneously produced at, most likely, different locations along the bow shock–magnetosheath region.

4. Summary and discussion

Using MEX/IMA, discrete foreshock-like O^+ was found just outside of the dayside bow shock with higher energy flux than the foreshock H^+. The acceleration of these O^+ started from inside the magnetosheath, gradually increasing in energy toward the solar wind region as a spatial structure, and this O^+ ion structure was observed extending more than 1500 km away from the bow shock. At slightly higher energy, foreshock H^+ were simultaneously observed at larger distances from the bow shock than the foreshock O^+, extending at least 3000 km from the bow shock where the IMA operation ended. Both the O^+ and H^+ flows are contained within limited directions without a large spread in angle (Fig. 4a), staying in the same direction for more than the distance of a proton gyroradius, indicating nearly field-aligned flow for the observed H^+. The flow angle between the directions of two species is about 50° (Fig. 3), with protons more anti-sunward than O^+ (Fig. 2).

The large contribution of O^+ to the foreshock population raises a question about the foreshock formation mechanism. The present example indicates that the local plasma (O^+) is able to form the main component of the foreshock ions and its morphology is closer to ordinary foreshock ions rather than the multiple reflection signature that are caused by specular reflection of solar wind at the bow shock. However, it is too early to conclude that the foreshock ions are formed by such a local acceleration because some foreshock populations contain alpha particles, indicating that they came from reflected solar wind (Fuselier and Thomsen, 1992). The energy–mass matrix in Fig. 4a shows also substantial counts in the He^{++} channel at nearly the same energy as foreshock H^+. Therefore, the mechanism(s) to produce the foreshock ions must explain both the local cold source (accelerated) and the solar wind (accelerated more than specular reflection).

Note that the narrowness of the observed foreshock H^+ by itself does not tell information about the spread of the H^+ direction at the source (bow shock) because only those ions that flow in nearly the field-aligned direction can reach a distance beyond one ion gyroradius from the bow shock. On the other hand, the flow direction of the very narrow He^{++} in Fig. 4a is slightly different from that of the foreshock H^+, as drawn in Fig. 3, and this could

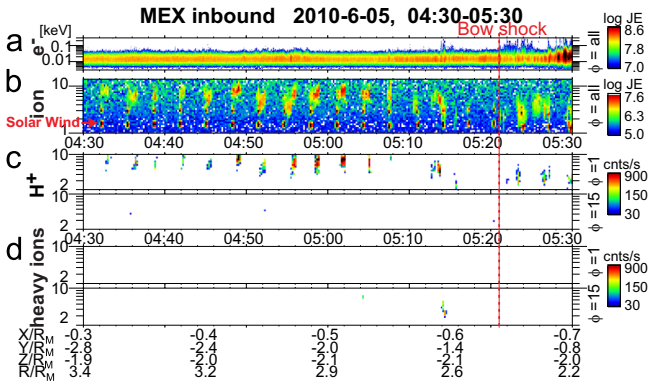

Fig. 6. Same format as Fig. 1 but for the 5 June 2010 foreshock event.

give some hint on the reflection at the bow shock. Although the distance from the bow shock where He^{++} is detected is comparable to the He^{++} gyroradius, it is still difficult to explain why there is such a wide angular separation in the flow direction between H^+ and He^{++} if the ejection angle from the bow shock is wide. Furthermore, the O^+ direction is very narrow and constant all the way from the magnetosheath to the solar wind region, indicating that these O^+ are flowing with small pitch angles and therefore are accelerated nearly along the field-aligned direction by a quasi-stationary mechanism.

Although the location of the O^+ acceleration is different from that of the solar wind H^+ reflection (cf. Fig. 5a), the observed energies of H^+ and O^+ in the foreshock are related. According to Fig. 1d, the acceleration of the O^+ data is equivalent to a 1 kV electric potential (slightly oriented anti-sunward with respect to the radial direction). If an acceleration equivalent to 1 keV is added to the specularly reflected solar wind H^+ (0.6 keV) in the same direction as O^+ acceleration, we expect about 1.3 keV H^+ flowing in oblique direction between radial and anti-sunward, as is observed in Fig. 1c. Thus, the observation suggests that the same acceleration mechanism (does not have to be potential acceleration) was most likely applied to both the cold O^+ in the magnetosheath and the reflected solar wind, as illustrated in Fig. 5b. In such a case, the O^+ direction and the H^+ direction are naturally different, and this acceleration is velocity independent (i.e., acceleration scenarios by Lorentz force only will be excluded).

The mechanism for the O^+ acceleration is an open question. There are many models and simulations of the solar wind reflection (e.g., Gosling et al., 1982; Burgess and Schwartz, 1984; Richer et al., 2012), but none of them predicted any test particle (O^+) to be accelerated in nearly constant and collimated direction as observed. If the O^+ acceleration of about 1 keV is related to the temporal and/or localized electric charging like the case for field-aligned potential acceleration, then the hybrid code simulations assuming quasi-neutrality are not adequate to study the observed phenomenon.

The existence of O^+ in the foreshock region with increasing energy outward from the bow shock also indicates the existence of dense cold O^+ in the bow shock, which has never been reported. The supply route of these O^+ ions is not clear but it is not likely that they come from (the temporal expansion of) the oxygen corona because such a scenario predicts a much lower count rate in the foreshock O^+ distribution in Fig. 1. Thus, the cold O^+ is probably transported from the ionosphere as cold dense ions through the route that the spacecraft did not traverse (cf. Fig. 2). We have no clue to the exact route of these planetary oxygen.

The O^+ foreshock observation opens up a new escape channel for planetary ions as cold bulk ions that are accelerated in the bow shock. Such a possibility has never been considered in past escape models (e.g., Yamauchi and Wahlund, 2007). If we do not seek a large-scale event like that shown in Fig. 1, discrete O^+ distributions are sometimes observed in the foreshock region. Fig. 6 shows one such example from 5 Jun 2010, where the spacecraft performed an inbound traversal at the flank of the bow shock. The solar wind is continuously observed until 05:26 UT without a reflection signature (Yamauchi et al., 2011). Inside the solar wind, isolated from the bow shock, foreshock H^+ is observed occupying a relatively narrow flow direction in a similar manner as Fig. 1. At the end of these foreshock ion observations (closest to the bow shock), a slightly different ion distribution from the main part of the foreshock population is observed at around 05:13 UT. The energy mass matrix (Fig. 4b) indicates that this signature contains a substantial amount of heavy ions, either O_2^+ or O^+.

Yamauchi et al (2011) surveyed the solar wind data between 2004 and 2005 for foreshock signatures using IMA data when IMA operated in the lowest mass-resolution mode (which is the most favorable mode for detecting protons), but find no foreshocks that were similar to those detected in the upstream of Venus bow shock by an identical instrument. Even extending the survey to the other mass-resolution modes, only few cases of weak signature are found over more than 1000 traversals during 2004–2005. However, when extending this survey to 2011, the foreshock ion signature was observed occasionally, particularly during 2008 and 2010 (IMA was not in a suitable observation mode during 2006). These two years are times when the solar EUV flux reaching Mars was minimum due to both the solar cycle and the Sun–Mars distance (Lundin et al., 2013). The solar EUV controls the cold ion density in the bow shock and solar wind through both the expansion of the exosphere and ionization of the exospheric hydrogen, as is statistically shown by Yamauchi et al. (2015). Therefore, the increased occurrence rate of foreshock signatures during 2008 and 2010 suggests that cold ions in the bow shock somewhat controls the foreshock formation, although we cannot suggest any solid mechanism for such relation.

Acknowledgment

Both IMA and ELS are part of the ASPERA-3 experiment on the ESA Mars Express spacecraft. We are indebted to all of the involved national agencies and to the European Space Agency for conducting the Mars Express program, especially the Swedish National Space Board, CNRS in France, and NASA (contract NASW-00003) in the USA. The lead author (MY) wishes to thank the social welfare (personal assistant) program in Sweden for providing assistance to physically disabled individuals which made it possible for him to conduct this research.

References

Asbridge, J.R., Bame, S.J., Strong, I.B., 1968. Outward flow of protons from the Earth's bow shock. J. Geophys. Res. 73, 5777–5782. http://dx.doi.org/10.1029/JA073i017p05777.

Barabash, S., Lundin, R., Andersson, H., Brinkfeldt, K., Grigoriev, A., Gunell, H., Holmström, M., Yamauchi, M., Asamura, K., Bochsler, P., Wurz, P., Cerulli-Irelli, R., Mura, A., Milillo, A., Maggi, M., Orsini, S., Coates, A.J., Linder, D.R., Kataria, D.O., Curtis, C.C., Hsieh, K.C., Sandel, B.R., Frahm, R.A., Sharber, J.R., Winningham, J.D., Grande, M., Kallio, E., Koskinen, H., Riihelä, P., Schmidt, W., Säles, T., Kozyra, J.U., Krupp, N., Woch, J., Livi, S., Luhmann, J.G., McKenna-Lawlor, S., Roelof, E.C., Williams, D.J., Sauvaud, J.-A., Fedorov, A., Thocaven, J.-J., 2006. The analyzer of space plasmas and energetic atoms (ASPERA-3) for the Mars Express mission. Sp. Sci. Rev. 126 (1–4), 113–164. http://dx.doi.org/10.1007/s11214-006-9124-8.

Burgess, D., Schwartz, S.J., 1984. The dynamics and upstream distributions of ions reflected at the Earth's bow shock. J. Geophys. Res. 89 (A9), 7407–7422. http://dx.doi.org/10.1029/JA089iA09p0740.

Dubinin, E., Lundin, R., Koskinen, H., Norberg, O., 1993. Cold ions at the Martian bow shock Phobos observations. J. Geophys. Res. 98, 5617–5623. http://dx.doi.org/10.1029/92JA02374.

Dubinin, E.M., Sauer, K., Delva, M., Grard, R., Livi, S., Lundin, R., Skalsky, A., Schwingenschuh, K., Szego, Trotignon, J.-G., 2000. Multi-instrument study of the upstream region near Mars: the Phobos-2 observations. J. Geophys. Res. 105 (A4), 7557–7571. http://dx.doi.org/10.1029/1999JA900400.

Eastwood, J.P., Lucek, E.A., Mazelle, C., Meziane, K., Narita, Y., Pickett, J., Treumann, R.A., 2005. The foreshock. Sp. Sci. Rev. 118, 41–94. http://dx.doi.org/10.1007/s11214-005-3824-3.

Edmiston, J.P., Kennel, C.F., Eichler, D., 1982. Escape of heated ions upstream of quasi-parallel shocks. Geophys. Res. Lett. 9 (5), 531–534. http://dx.doi.org/10.1029/GL009i005p00531.

Fedorov, A., Budnik, E., Sauvaud, J.-A., Mazelle, C., Barabash, S., Lundin, R., Acuna, M., Holström, M., Grigoriev, A., Yamauchi, M., Andersson, H., Thocaven, J.J., Winningham, D., Frahm, R., Sharber, J.R., Scherrer, J., Coates, A.J., Linder, D.R., Kataria, D.O., Kallio, E., Koskinen, H., Säles, T., Riihelä, P., Schmidt, W., Kozyra, J., Luhmann, J., Roelof, E., Williams, D., Livi, S., Curtis, C.C., Hsieh, K.C., Sandel, B.R., Grande, M., Carter, M., McKenna-Lawler, S., Orsini, S., Cerulli-Irelli, R., Maggi, M., Wurz, P., Bochsler, P., Krupp, N., Woch, J., Fränz, M., Asamura, K., Dierker, C., 2006. Structure of the Martian wake. Icarus 182 (2), 329–336. http://dx.doi.org/10.1016/j.icarus.2005.09.021.

Frahm, R.A., Winningham, J.D., Sharber, J.R., Scherrer, J.R., Jeffers, S.J., Coates, A.J., Linder, D.R., Kataria, D.O., Lundin, R., Barabash, S., Holmström, M., Andersson, H., Yamauchi, M., Grigoriev, Kallio, E., Säles, T., Riihelä, P., Schmidt, W., Koskinen, H., Kozyra, J.U., Luhmann, J.G., Roelof, E.C., Williams, D.J., Livi, S., Curtis, C.C., Hsieh, K.C., Sandel, B.R., Grande, M., Carter, M., Sauvaud, J.-A., Fedorov, A., Thocaven, J.-J., McKenna-Lawler, S., Orsini, S., Cerulli-Irelli, R., Maggi, M., Wurz, P., Bochsler, P., Krupp, N., Woch, J., Fränz, M., Asamura, K., Dierker, C., 2006a. Carbon dioxide photoelectron energy peaks at Mars. Icarus 182, 371–382. http://dx.doi.org/10.1016/j.icarus.2006.01.014.

Frahm, R.A., Sharber, J.R., Winningham, J.D., Wurz, P., Liemohn, M.W., Kallio, E., Yamauchi, M., Lundin, R., Barabash, S., Coates, A.J., Linder, D.R., Kozyra, J.U., Holmström, M., Jeffers, S.J., Andersson, H., McKenna-Lawler, S., 2006b. Locations of atmospheric photoelectron energy peaks within the Mars environment. Sp. Sci. Rev. 126, 389–402. http://dx.doi.org/10.1007/s11214-006-9119-5.

Fuselier, S.A., Thomsen, M.F., 1992. He^{2+} in field aligned beams: ISEE results. Geophys. Res. Lett. 19 (5), 437–440. http://dx.doi.org/10.1029/92GL00375.

Gosling, J.T., Asbridge, J.R., Bame, S.J., Paschmann, G., Sckopke, N., 1978. Observations of two distinct populations of bow shock ions in the upstream solar wind. Geophys. Res. Lett. 5 (11), 957–960. http://dx.doi.org/10.1029/GL005i011p00957.

Gosling, J.T., Thomsen, M.F., Bame, S.J., Feldman, W.C., Paschmann, G., Sckopke, N., 1982. Evidence for specularly reflected ions upstream from the quasi-parallel bow shock. Geophys. Res. Lett. 9 (12), 1333–1336. http://dx.doi.org/10.1029/GL009i012p01333.

Krimigis, S.M., Sibeck, D.G., McEntire, R.W., 1986. Magnetospheric particle injection and the upstream ion event of September 5, 1984. Geophys. Res. Lett. 13 (13), 1376–1379. http://dx.doi.org/10.1029/GL013i013p01376.

Kucharek, H., Möbius, E., Scholer, M., Mouikis, C., Kistler, L.M., Horbury, T., Balogh, A., Rème, H., Bosqued, J.M., 2004. On the origin of field-aligned beams at the quasi-perpendicular bow shock: multi-spacecraft observations by Cluster. Ann. Geophys. 22, 2301–2308. http://dx.doi.org/10.5194/angeo-22-2301-2004.

Lundin, R., Barabash, S., Holmström, M., Nilsson, H., Futaana, Y., Ramstad, R., Yamauchi, M., Dubinin, E., Fraenz, M., 2013. Solar cycle effects on the ion escape from Mars. Geophys. Res. Lett. 40 (23), 6028–6032. http://dx.doi.org/10.1002/2013GL058154.

Mazelle, C., Meziane, K., LeQuéau, D., Wilber, M., Eastwood, J.P., Rème, H., Sauvaud, J.-A., Bosqued, J.M., Dandouras, I., McCarthy, M., Kistler, L.M., Klecker, B., Korth, A., Bavassano-Cattaneo, M.B., Pallocchia, G., Lundin, R., Balogh, A., 2003. Production of gyrating ions from nonlinear wave-particle interaction upstream from the Earth's bow shock: a case study from Cluster-CIS. Planet. Sp. Sci. 51, 785–795. http://dx.doi.org/10.1016/j.pss.2003.05.002.

Meziane, K., Mazelle, C., Wilber, M., LeQuéau, D., Eastwood, J.P., Rème, H., Dandouras, I., Sauvaud, J.A., Bosqued, J.M., Parks, G.K., Kistler, L.M., McCarthy, M., Klecker, B., Korth, A., Bavassano-Cattaneo, M.-B., Lundin, R., Balogh, A., 2004. Bow shock specularly reflected ions in the presence of lowfrequency electromagnetic waves: a case study. Ann. Geophys. 22, 2325–2335. http://dx.doi.org/10.5194/angeo-22-2325-2004.

Möbius, E., Hovestadt, D., Klecker, B., Scholer, M., Ipavich, F.M., Carlson, C.W., Lin, R.P., 1986. A burst of energetic O^+ ions during an upstream particle event. Geophys. Res. Lett. 13 (13), 1372–1375. http://dx.doi.org/10.1029/GL013i013p01372.

Paschmann, G., Sckopke, N., Asbridge, J.R., Bame, S.J., Gosling, J.T., 1980. Energization of solar wind ions by reflection from the Earth's bow shock. J. Geophys. Res. 85, 4689–4693. http://dx.doi.org/10.1029/JA085iA09p04689.

Richer, E., Chanteur, G.M., Modolo, R., Dubinin, E., 2012. Reflection of solar wind protons on the Martian bow shock: investigations by means of 3-dimensional simulations. Geophys. Res. Lett. 39, L17101. http://dx.doi.org/10.1029/2012GL052858.

Sarris, E.T., Anagnostopoulos, G.C., Krimigis, S.M., 1987. Simultaneous measurements of energetic ion (50 keV and above) and electron (220 keV and above) activity upstream of Earth's bow shock and inside the plasma sheet - Magnetospheric source for the November 3 and December 3, 1977 upstream events. J. Geophys. Res. 92 (A11), 12083–12096. http://dx.doi.org/10.1029/JA092iA11p12083.

Sibeck, D.G., McEntire, R.W., Krimigis, S.M., Baker, D.N., 1988. The magnetosphere as a sufficient source for upstream ions on November 1, 1984. J. Geophys. Res. 93 (A12), 14328–14342. http://dx.doi.org/10.1029/JA093iA12p14328.

Tanaka, M., Goodrich, C.C., Winske, D., Papadopoulos, K., 1983. A source of the backstreaming ion beams in the foreshock region. J. Geophys. Res. 88, 3046–3054. http://dx.doi.org/10.1029/JA088iA04p03046.

Yamauchi, M., Futaana, Y., Fedorov, A., Dubinin, E., Lundin, R., Sauvaud, J.-A., Winningham, D., Frahm, R., Barabash, S., Holmström, M., Woch, J., Fraenz, M., Budnik, E., Borg, H., Sharber, J.R., Coates, A.J., Soobiah, Y., Koskinen, H., Kallio, E., Asamura, K., Hayakawa, H., Curtis, C., Hsieh, K.C., Sandel, B.R., Grande, M., Grigoriev, A., Wurz, P., Orsini, S., Brandt, P., McKenna-Lawler, S., Kozyra, J., Luhmann, J., 2006. IMF direction derivation from cycloid-like ion distributions observed by Mars Express. Sp. Sci. Rev. 126 (1–4), 239–266. http://dx.doi.org/10.1007/s11214-006-9090-1.

Yamauchi, M., Wahlund, J.-E., 2007. Role of the ionosphere for the atmospheric evolution of planets. Astrobiol. J. 7 (5), 783–800. http://dx.doi.org/10.1089/ast.2007.0140.

Yamauchi, M., Futaana, Y., Fedorov, A., Kallio, E., Frahm, R.A., Lundin, R., Sauvaud, J.-A., Winningham, D.J., Barabash, S., Holmström, M., 2008. Advanced method to derive the IMF direction near Mars from cycloidal proton distributions. Planet. Sp. Sci. 56 (8), 1145–1154. http://dx.doi.org/10.1016/j.pss.2008.02.012.

Yamauchi, M., Futaana, Y., Fedorov, R.A., Frahm, R.A., Winningham, J.D., Dubinin, E., Lundin, R., Barabash, S., Holmström, M., Mazelle, C., Sauvaud, J.-A., Zhang, T.L., Baumjohann, W., Coates, A.J., Fraenz, M., 2011. Comparison of accelerated ion populations observed upstream of the bow shocks at Venus and Mars. Ann. Geophys. 29 (3), 511–528. http://dx.doi.org/10.5194/angeo-29-511-2011.

Yamauchi, M., Futaana, Y., Fedorov, A., Frahm, R.A., Dubinin, E., Lundin, R., Sauvaud, J.-A., Winningham, J.D., Barabash, S., Holmstrom, M., 2012. Ion acceleration by multiple reflections at Martian bow shock. Earth Planets Sp. 64 (2), 61–71. http://dx.doi.org/10.5047/eps.2011.07.007 2012.

Yamauchi, M., Hara, T., Lundin, R., Dubinin, E., Fedorov, A., Sauvaud, J.-A., Frahm, R.A., Ramstad, R., Futaana, Y, Holmström, M. and Barabash, S., Strong seasonal variation of Martian pick-up ions and reflected ions, Planet Sp. Sci. (submitted for publication, for the same issue) ⟨http://www.irf.se/~yamau/papers/pickup_season_revised.pdf⟩.